

The unusual emission line spectrum of I Zw 1

M.-P. Véron-Cetty¹, M. Joly² and P. Véron¹ *

¹ Observatoire de Haute Provence, CNRS, F-04870 Saint-Michel l'Observatoire, France

e-mail: mira.veron@oamp.fr; philippe.veron@oamp.fr

² Observatoire de Paris-Meudon, 5 place J. Janssen, F-92195 Meudon, France

e-mail: Monique.Joly@obspm.fr

Received ; accepted

Abstract. Most Seyfert 1s show strong Fe II lines in their spectrum having the velocity and width of the broad emission lines. To remove the Fe II contribution in these objects, an accurate template is necessary. We used very high signal-to-noise, medium resolution archive optical spectra of I Zw 1 to build such a template. I Zw 1 is a bright narrow-line Seyfert 1 galaxy. As such it is well suited for a detailed analysis of its emission line spectrum. Furthermore it is known to have a very peculiar spectrum with, in addition to the usual broad and narrow line regions, two emission regions emitting broad and blue shifted [O III] lines making it a peculiarly interesting object. While analysing the spectra, we found that the narrow-line region is, unlike the NLR of most Seyfert 1 galaxies, a very low excitation region dominated by both permitted and forbidden Fe II lines. It is very similar to the emission spectrum of a blob in η Carinae which is a low temperature ($T_e \sim 6\,500$ K), relatively high density ($N_e = 10^6 \text{ cm}^{-3}$) cloud. The Fe II lines in this cloud are mainly due to pumping via the stellar continuum radiation field (Verner et al. 2002). We did not succeed in modelling the spectrum of the broad-line region, and we suggest that a non radiative heating mechanism increases the temperature in the excited H I region, thus providing the necessary additional excitation of the Fe II lines. For the low-excitation narrow-line region, we are able to settle boundaries to the physical conditions accounting for the forbidden and permitted Fe II lines ($10^6 < N_e < 10^7 \text{ cm}^{-3}$; $10^{-6} < U < 10^{-5}$).

Key words. galaxies: Seyfert–galaxies: individual: I Zw 1

October 31, 2018

1. Introduction

I Zw 1 is a compact galaxy discovered by Zwicky (1964; 1971). Its redshift, as determined from neutral hydrogen emission, is $z=0.0611$ (Condon et al. 1985).

Its spectrum has broad hydrogen and Fe II emission lines (Sargent 1968). Phillips (1976) showed the existence of two separate redshift systems for the emission lines originating in the nucleus. The majority of the lines belongs to the highest redshift system ($z=0.0608$); most of the features in this system can be identified with Fe II or H I lines, but emission from He I, Ca II, Na I D, [N II], [S II] and [O I] is also apparently present. The lines detected at the smaller redshift ($z=0.0587$) are [O III] $\lambda\lambda 4959, 5007$ and [Ne III] $\lambda\lambda 3869, 3967$. Oke & Lauer (1979) confirmed the existence of two redshift systems; they found evidence for an additional component in the [O III] and [Ne III]

lines with an even smaller redshift ($z=0.0548$). The low-ionization forbidden lines, although having the same redshift as the broad H and Fe II lines, have a much narrower width ($\sim 300 \text{ km s}^{-1}$ FWHM), constituting a separate system (Van Groningen 1993).

The emission line spectrum of I Zw 1 is therefore quite complex with at least four distinct systems.

Both Fe II and Fe III permitted emission lines have been detected in a high signal to noise ratio UV (1100–3800 Å) spectrum of I Zw 1 (Laor et al. 1997). Several Fe II lines are emitted from levels higher than 10 eV above ground level. The Fe III line widths distribution is bimodal, with two maxima centered at ~ 330 and 780 km s^{-1} FWHM. Most of the UV Fe II emission lines are narrow (FWHM $\sim 400 \text{ km s}^{-1}$). The broader lines are likely coming from the region emitting the broad Balmer and optical Fe II lines, while the narrower ones must come from the region emitting the narrow low-excitation forbidden lines (Vestergaard & Wilkes 2001).

Send offprint requests to: P. Véron

* Based on WHT and AAT spectra retrieved from the ING and AAT archives.

Both the continuum and the broad emission lines have been shown to be variable over a time scale of a few years, although with a rather low amplitude, not exceeding a few tenths of a magnitude (Peterson et al. 1984; Winkler 1997; Giannuzzo et al. 1998).

The nuclear region of IZw 1 is currently undergoing vigorous star formation, the stellar component being strongly affected by extinction (Eckart et al. 1994).

Boroson & Green (1992) have built a template Fe II spectrum from the observed spectrum of IZw 1. This template has since been universally used by all authors studying the broad emission line spectra of Seyfert 1 galaxies.

However it appears that the various UV multiplets in IZw 1 may not vary by the same amount when the continuum varies (Vestergaard & Wills 2001) and that the various optical multiplets have not the same relative intensities in different objects, for instance in IZw 1 and Akn 564 (van Groningen 1993).

When trying to check if a single Fe II template could allow the removal of the broad Fe II emission in all Seyfert 1 galaxies, we felt the need to use a more accurate IZw 1 template than the one built according to the Boroson & Green precepts. To do so, we have used three very high signal-to-noise ratio spectra of IZw 1 taken either from the ING or the AAT data archives.

2. The spectra and their reduction

2.1. The WHT spectra

2.1.1. The red spectrum

IZw 1 has been observed on 1998, October 1 and 3 (for 2×4000 and 2×2400 sec respectively) at the Observatorio de los Muchachos on the island of La Palma, with the ISIS dual beam spectrograph of the 4.2-m William Herschel Telescope (WHT) (Smith et al. 2002). The red arm of the spectrograph was used with a $1024 \times 1024 \times 24 \times 24 \mu\text{m}$ pixel Tektronic CCD detector and the R316R (316 lines mm^{-1}) grating, giving a wavelength range of $\sim 1500 \text{ \AA}$ ($6040\text{--}7535 \text{ \AA}$) and a dispersion of 62 \AA mm^{-1} ($1.5 \text{ \AA pixel}^{-1}$). The slit width was $1''.2$ (*i.e.* $75 \mu\text{m}$ or 3 pixels on the detector). The FWHM of the arc lines varied from 3.5 to 4.1 \AA from the red to the blue end of the spectrum. A comb dekker was used to prevent overlapping of the two sets of spectra produced by the beam-splitting calcite slab. The dekker apertures were $2''.7$, separated by $18''$. The object was observed using the standard spectropolarimetry procedure of taking equal exposures at half-wave plate angles of 0° , 22.5° , 45° and 67.5° . Five columns were extracted, corresponding to $1''.8$ on the sky. Observations of the spectrophotometric standard EG 247 were obtained to allow flux calibration of the spectra and the removal of atmospheric absorption features. Wavelength calibration was achieved via observations of a CuNe lamp.

In the present study, we used only the October 1 spectrum.

2.1.2. The blue spectrum

IZw 1 was observed on 1998, December 16 with the WHT telescope and the blue arm of the ISIS dual beam spectrograph in long slit mode with a EEV12 $2048 \times 4100 \times 13.5 \times 13.5 \mu\text{m}$ pixel CCD detector. The R300B grating (300 lines mm^{-1}) was used, giving a useful wavelength range of 2250 \AA ($3750\text{--}6000 \text{ \AA}$) and a dispersion of 64 \AA mm^{-1} ($0.86 \text{ \AA pixel}^{-1}$). The slit width was $1''.2$ (*i.e.* $80 \mu\text{m}$ or 6 pixels on the detector). The FWHM of the arc lines was $\sim 4 \text{ \AA}$. Two exposures were obtained of 600 and 1800 sec respectively. Fifteen columns were extracted, corresponding to $3''.0$ on the sky. Observations of the spectrophotometric standard BD+28.4211 were obtained. The FWHM of the spectra was 9.2 and 8.3 pixels ($1''.85$ and $1''.65$) for IZw 1 and the standard star respectively. Wavelength calibration was achieved via observations of a CuAr lamp.

2.2. The AAT spectrum

IZw 1 was observed on 1997, August 2 (for 4×1200 sec) at the 3.9-m Anglo-Australian Telescope with the Royal Greenwich Observatory spectrograph in conjunction with the waveplate polarimeter with a $1024 \times 1024 \times 24 \times 24 \mu\text{m}$ pixel Tektronic CCD detector (Smith et al. 2002). The 270R (270 lines mm^{-1}) grating was used, giving a wavelength range of $\sim 3450 \text{ \AA}$ ($4350\text{--}7800 \text{ \AA}$) and a dispersion of 140 \AA mm^{-1} ($3.4 \text{ \AA pixel}^{-1}$). The slit width was $2''.0$ (*i.e.* $58 \mu\text{m}$ or 2.4 pixels on the detector). A two-hole dekker with $2.7 \times 2.7 \text{ arcsec}^2$ apertures separated by $27''$ was used, with the object located in one aperture and the other providing a sky measurement. The FWHM of the arc lines were $\sim 8.5 \text{ \AA}$. Five columns were extracted, corresponding to $4''.0$ on the sky. Observations of the spectrophotometric standard HD 140283 were obtained. Wavelength calibration was achieved via observations of a CuNe lamp.

The AAT spectrum of IZw 1 is shown in Fig. 1.

2.3. Analysis

All spectra have been deredshifted using $z=0.0603$. We have tried to identify all emission features. To get a good fit¹, four major line systems with different line velocity and width were required in agreement with previous studies: a relatively broad Lorentzian system L1, two Gaussian “narrow” high-excitation line systems N1 and N2 and a third narrow low-excitation line system N3, taken as reference for the velocities. In each system all the lines have been forced to have the same velocity and width. Figures 2 and 3 show the best fits obtained for the red and blue WHT spectra respectively.

¹ The fits were done using a software originally written by E. Zuiderwijk and described in Véron et al. (1980).

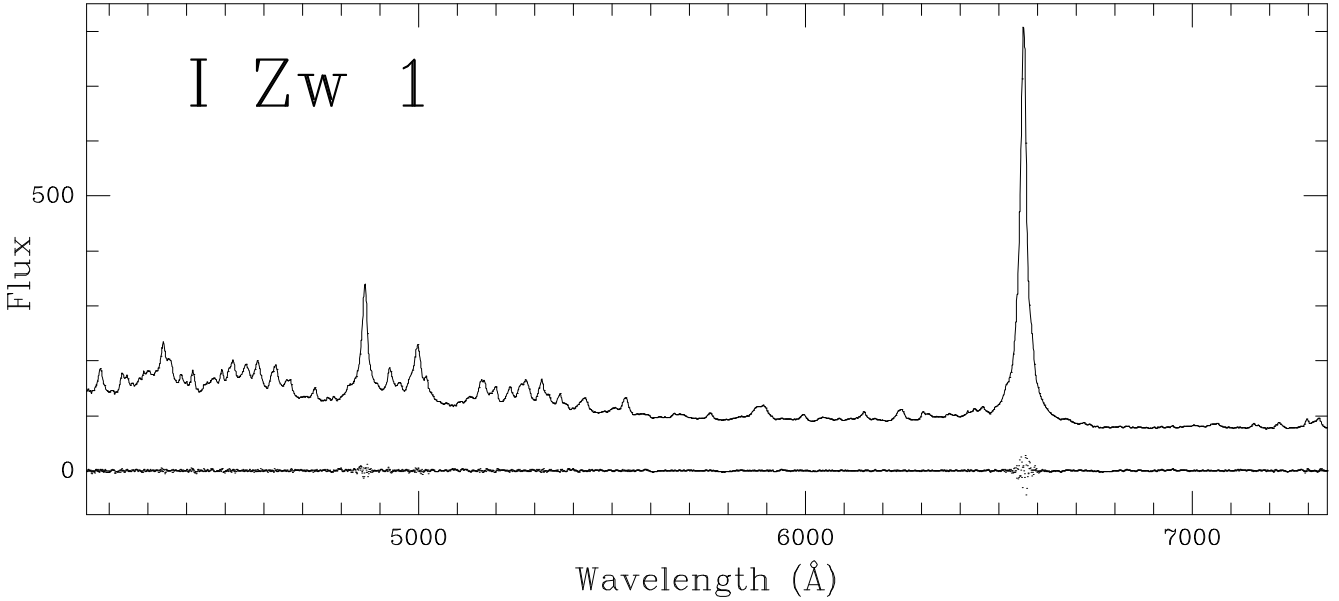


Fig. 1. The deredshifted AAT spectrum of IZw 1 with the residuals. The fit is not shown. The fluxes are in units of $10^{-16} \text{ erg cm}^{-2} \text{ Å}^{-1} \text{ s}^{-1}$.

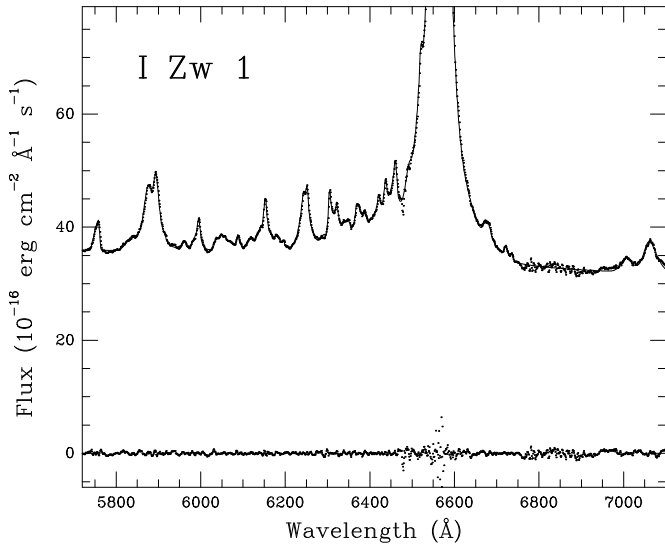


Fig. 2. The deredshifted red WHT spectrum of IZw 1 (dots), the best fit and the residuals.

2.3.1. The broad line system L1

In system L1 ($V = -150 \text{ km s}^{-1}$; 1100 km s^{-1} FWHM), we found a number of permitted Fe II lines and a few other lines listed in Table 1, including Balmer, He I, Si II, Ti II and Na I D lines. Table A.1 gives the list of all lines included in the fit with their intensities.

To get a good fit we had to add to the Balmer lines another very broad Gaussian component (FWHM = 5600 km s^{-1}) which means that the line profile in the broad

line region is more complex than a single Lorentzian. We have previously observed a similar complexity in the case of HS 0328+05 (Véron et al. 2002).

Weak permitted Ti II lines frequently occur in various types of emission line spectra, especially those with strong bright Fe II lines. More than 100 Ti II lines have been measured in the very peculiar spectrum of XX Ophiuci (Merrill 1951; 1961).

It turns out that, on the AAT spectrum on which both $H\alpha$ and $H\beta$ are visible, the Lorentzian components of these two lines do not have the same velocity; $H\beta$ is blueshifted with respect to $H\alpha$ by about 85 km s^{-1} . The optical-UV continuum of IZw 1 is significantly redder than observed in typical QSOs; the reddening was estimated to be $E(B-V) \sim 0.2$ (Laor et al. 1997). Wills (1983) used $E(B-V) = 0.21$. From the comparison of the intensities of the O I $\lambda 1304$ and $\lambda 8446$ lines, Rudy et al. (2000) have estimated the reddening of the broad line region to be $E(B-V) \sim 0.19$. These values are substantially larger than the reddening in the direction of IZw 1 due to the Milky Way as determined from the IR images of Schlegel et al. (1998), *i.e.* $E(B-V) = 0.07$, or from the Galactic hydrogen column density observed by Stark et al. (1992) *i.e.* $E(B-V) = 0.105$, so the broad line region probably suffers a significant intrinsic reddening of the order of $E(B-V) \sim 0.09$ - 0.13 (Rudy et al. 2000).

If the region emitting the broad lines is not uniformly covered by the absorbing dust, but if the receding part of the emitting cloud suffers an extinction stronger than the approaching part, $H\beta$ would appear blueshifted with respect to $H\alpha$, as observed. To correct for this effect when

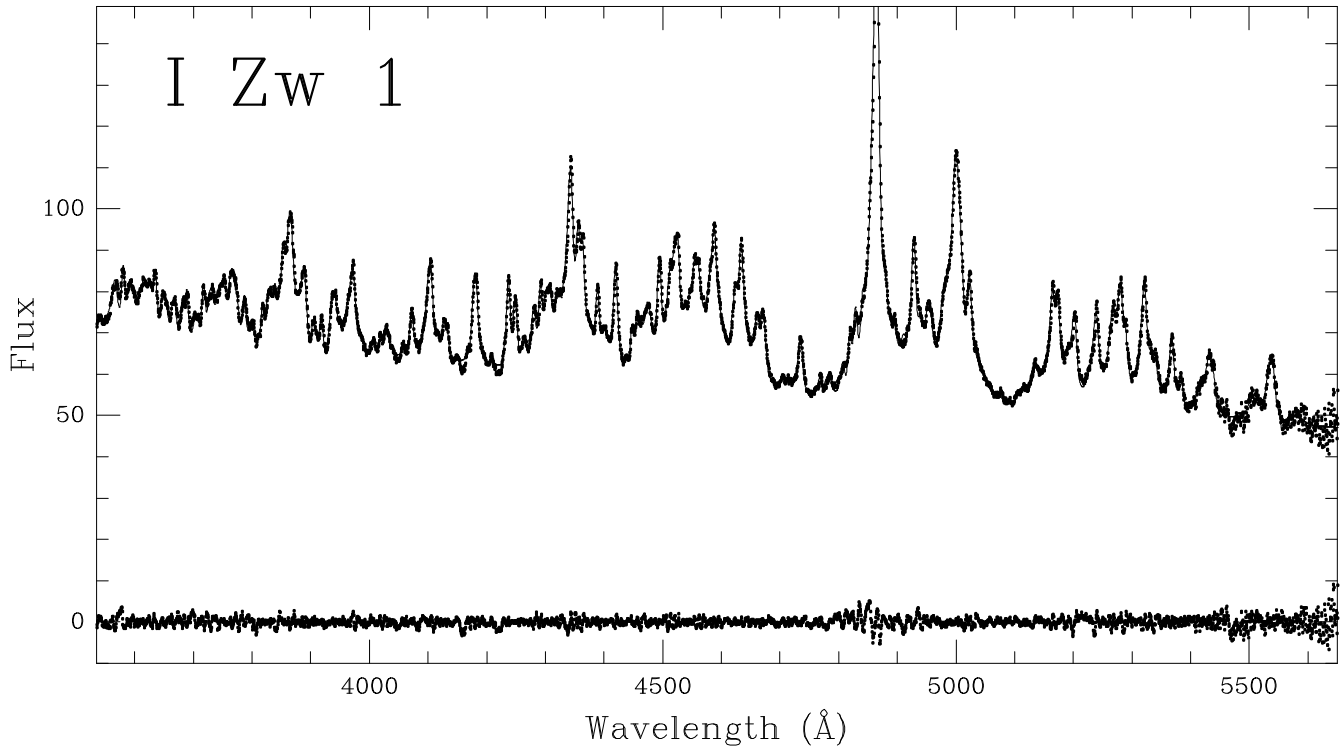


Fig. 3. The deredshifted blue WHT spectrum of IZw 1 (dots), the best fit and the residuals. The fluxes are in units of $10^{-16} \text{ erg cm}^{-2} \text{ Å}^{-1} \text{ s}^{-1}$.

fitting the AAT spectrum, we assumed that the broad lines in the blue part of the spectrum ($\lambda < 5000 \text{ Å}$) have a different redshift than the lines in the red part.

Due to the complexity of the Balmer line profiles and the relative weakness of the high order Balmer lines, we have set the intensity of these lines relative to $H\beta$ (except for $H\alpha$) to values determined by trial and errors. We could not use the Balmer decrements for the radiative recombination case B, reddened by the observed value of $E(B-V)$ for the following reason. While in most Seyfert 1 galaxies, the $H\gamma/H\beta$ and $H\delta/H\beta$ ratios are compatible with the values expected for a recombination spectrum affected by reddening, the points representing the $H\alpha/H\beta$ vs $H\gamma/H\beta$ line ratios are scattered and do not show any sign of correlation (Rafanalli 1985). In four observed radio galaxies, the Balmer decrement is much steeper than the recombination decrement $H\alpha/H\beta/H\gamma \sim 2.9/1.0/0.47$ and cannot be matched to this recombination decrement with any assumed amount of standard interstellar reddening (Osterbrock et al. 1976). In a sample of 24 Seyfert 1/QSOs, Neugebauer et al. (1979) found that the average ratio of intensities of $H\alpha/H\beta$ is 3.65 with a range from 2.2 to 4.9, with only one object having a ratio less than the case B radiative recombination value of 2.8. Wu et al. (1980) also found, in a sample of 13 Seyfert 1 galaxies, that the intrinsic value of the $H\alpha/H\beta$ ratio is >2.8 . Moreover a fraction of all Seyfert 1 galaxies, called Seyfert 1.8 and 1.9, have a very steep Balmer decrement ($H\alpha/H\beta$) which are not always due

to a high reddening as shown by the observation of the $\text{Pa } \alpha$ line which, in some of these objects, is too weak to be explained by the reddening hypothesis (Goodrich 1990). In the Seyfert 1.9 galaxy VZw 317, the Balmer decrement is very steep ($H\alpha/H\beta \sim 15.1$), but the $\text{Pa } \alpha$ line is less than one-sixth the case B value modified by reddening so, in this case, reddening alone cannot account for the observed line ratio. Radiative transfer effects are probably the dominant factor in producing the observed broad-line $H\alpha/H\beta$ ratio (Collin-Souffrin et al. 1982; Rudy et al. 1983).

In system L1 the helium emission does not appear to be very strong. No He II lines were detected and the only He I lines which have been positively identified by Phillips (1976) or Oke & Lauer (1979) are $\lambda 5876$ and $\lambda 7065$. In addition to these two lines, we also observed $\lambda 3705$, $\lambda 4026$ and $\lambda 6678$.

To identify the Fe II lines, we made use of the line lists of Hirata & Horaguchi (1995) and van Hoof (1996). Five of the multiplets we observed, m. 26, 35, 43, 46 and 55, are intercombination multiplets and therefore should be weak; we note however that, in XX Ophiuci, Merrill (1951) has observed lines from all of them (m. 43, 46 and 55 with a substantial intensity), and that both Phillips (1976) and Oke & Lauer (1979) observed lines from these three multiplets in IZw 1. Joly (1988) has shown that intercombination multiplets such as m. 35 can be strong when the optical thickness is large.

Table 1. Emission lines other than Fe II identified in the Lorentzian system L1 of the spectrum of IZw 1 from 3535 to 7300 Å. Col. 1: line, col. 2: wavelength, cols. 3 and 4: observed dereddened (using $E(B-V)=0.20$) intensities relative to $H\beta$ ($F(H\beta)=3.8\times 10^{-13}$ and 10.3×10^{-13} erg cm $^{-2}$ s $^{-1}$ for the WHT and AAT spectra respectively). An "h" in col. 3 means that the line is outside the observed spectral range.

Line	λ (Å)	AAT	WHT
H α	6562.8	2.51	3.70
H γ	4340.4	0.42	0.42
H δ	4101.7	h	0.22
H ϵ	3970.1	h	0.13
H 8	3889.1	h	0.08
H 9	3835.4	h	0.06
He I 25	3705.0	h	0.05
He I 18	4026.4	h	0.08
He I 11	5875.7	0.08	0.11
He I 46	6678.1	0.04	0.07
He I 10	7065.4	0.02	0.05
Na I D	5889.9	0.04	0.04
Na I D	5895.9	0.07	0.11
Ti II 72	3741.6	h	0.07
Ti II 50	4563.8	0.08	0.14
Ti II 50	4590.0	0.07	0.13
Ti II 70	5188.7	0.06	0.06
Si II 5	5041.1	0.03	0.05
Si II 5	5056.4	0.03	0.03
Si II 8	5827.8	0.02	0.02
Si II 8	5846.1	0.01	0.02
Si II 8	5868.4	0.04	0.05
Si II 2	6347.1	0.03	0.04
Si II 2	6371.4	0.02	0.03

Twenty seven of the observed Fe II lines are of high-excitation, their upper level being more than 6 eV above ground level. They are listed in Table 2. Six of them originate from the same upper level c^4D at ~ 7.48 eV, while seven come from a single other level $4d^4F$ at ~ 13.25 eV.

2.3.2. The high-excitation "narrow line" systems N1 and N2

These two systems have relatively broad and blueshifted emission lines ($V=-1\,450$ km s $^{-1}$, $1\,900$ km s $^{-1}$ FWHM for N1 and $V=-500$ km s $^{-1}$, 920 km s $^{-1}$ FWHM for N2), in agreement with Oke & Lauer (1979) (who also observed, in system N2, [O III] $\lambda 4363$ which we failed to detect). The lines observed in these systems are [O III] $\lambda\lambda 4959, 5007$, [Ne III] $\lambda\lambda 3869, 3967$, [N II] $\lambda\lambda 6548, 6583$ and in addition, in system N1, [Fe VII] $\lambda 6085$ and [S II] $\lambda\lambda 6716, 6731$. In the fit the line ratio $\lambda 3967/\lambda 3869$ has been set to its theoretical value of 0.31 (Galavis et al. 1997). Moreover, due to the relative weakness of the two systems compared to L1 and N3, we have set the ratio $\lambda 6583/H\alpha$ to 1.0 (the mean value observed in AGN) and $H\alpha/H\beta$ to 3.36. The line intensities

Table 2. Observed high-excitation Fe II lines in the spectrum of IZw 1 (system L1). Col. 1: wavelength, col. 2: upper level energy, col. 3: multiplet number, col. 4: transition, cols. 5 and 6: observed intensities relative to $H\beta$, corrected for a reddening of $E(B-V)=0.2$. An "h" in column 5 or 6 means that the line is outside the observed spectral range while an "n" means that it has not been detected.

λ (Å)	ul(eV)	m.	Transition	AAT	WHT
3564.53	7.63	113	$c^2G_{9/2}-z^4I_{9/2}$	h	0.11
3589.48	10.72		$d^2G_{9/2}-u^2F_{7/2}$	h	0.11
3614.87	7.58	112	$c^2G_{7/2}-z^4H_{7/2}$	h	0.12
3627.17	9.37	193	$d^2D_{5/2}-w^2F_{7/2}$	h	0.11
3649.39	12.39		$w^4D_{3/2}-f^4F_{3/2}$	h	0.08
3732.88	10.46		$d^4P_{1/2}-v^2D_{3/2}$	h	0.08
4093.66	10.60		$z^4G_{5/2}-e^4G_{7/2}$	h	0.06
4403.03	10.52		$y^4F_{9/2}-e^4G_{11/2}$	0.07	0.09
5030.64	12.75		$e^6F_{9/2}-4[5]_{9/2}$	0.08	0.11
5505.26	9.90		$y^4D_{7/2}-e^4D_{5/2}$	0.07	0.07
5738.18	13.25		$p^6P_{5/2}-4d^4F_{5/2}$	n	0.01
5955.51	9.96	217	$x^4D_{1/2}-e^4D_{1/2}$	0.01	0.02
6157.12	13.25		$p^4S_{3/2}-4d^4F_{5/2}$	0.02	0.04
6317.99	7.47		$z^4D_{7/2}-c^4D_{7/2}$	0.04	0.05
6336.95	13.25		$p^4F_{5/2}-4d^4F_{3/2}$	0.04	0.04
6385.45	7.49		$z^4D_{5/2}-c^4D_{3/2}$	0.05	0.05
6402.90	6.73		$z^6D_{7/2}-b^4G_{9/2}$	0.01	0.02
6442.95	7.47		$z^4F_{7/2}-c^4D_{7/2}$	0.02	0.02
6491.28	7.49		$z^4D_{3/2}-c^4D_{5/2}$	0.04	0.07
6500.63	9.78		x^4D-e^6D	0.03	0.06
6598.30	7.49		$z^4F_{3/2}-c^4D_{3/2}$	0.14	0.21
6623.07	7.49		$z^4F_{3/2}-c^4D_{1/2}$	0.03	0.06
6644.25	12.37		e^6G-^2G	0.02	0.03
6993.43	13.23		$v^4F_{9/2}-4d^4F_{9/2}$	0.02	0.01
7008.69	13.25		$u^2G_{7/2}-4d^4F_{5/2}$	0.02	0.03
7054.53	13.25		$u^2D_{5/2}-4d^4F_{5/2}$	0.04	0.05
7080.47	13.23		$u^2G_{7/2}-4d^4F_{9/2}$	n	0.02

relative to $H\beta$ in these two systems are given in Tables 3 and 4 respectively.

Schinnerer et al. (1998) have observed in the nucleus of IZw 1 two coronal lines: [Si IV] $\lambda 1.962\mu m$ and [Al IX] $\lambda 2.040\mu m$, blueshifted by $1\,350$ km s $^{-1}$ relative to the hydrogen recombination lines; they must originate from these two regions.

These two systems are somewhat similar to those observed in the spectrum of the compact radio source, Seyfert 2 galaxy PKS 1345+12 (Holt et al. 2003). In this object, the [O III] lines have been fitted with three Gaussian components, two of which being blueshifted and relatively broad (-402 km s $^{-1}$, $1\,255$ km s $^{-1}$ FWHM and $-1\,980$ km s $^{-1}$, $1\,944$ km s $^{-1}$ FWHM respectively). This blue shifted material was suggested to represent material in outflow from the nucleus. This situation is similar to that observed in another flat radio spectrum Seyfert 2 galaxy, PKS 1549-79 (Tadhunter et al. 2001).

Table 3. High excitation system N1. Col. 1: line, col. 2: wavelength, cols. 3 and 4: observed intensities relative to $H\beta$. The $H\beta$ flux is equal to 1.8 and 1.0×10^{-14} erg s $^{-1}$ cm $^{-2}$ in the AAT and WHT spectra respectively. An "h" in column 3 means that the line is outside the observed spectral range while an "n" means that it has not been detected.

Line	λ (Å)	AAT	WHT
$H\beta$	4861.30	1.00	1.00
$H\alpha$	6562.80	3.36	3.37
[O III]	4958.90	3.40	3.40
[O III]	5006.80	10.30	10.30
[Ne III] 1F	3868.74	h	4.04
[Ne III] 1F	3967.51	h	1.29
[Fe VII]	6085.50	0.84	0.88
[N II]	6548.10	1.14	1.14
[N II]	6583.40	3.37	3.38
[S II]	6716.40	n	0.12
[S II]	6730.80	n	0.10

Table 4. High excitation system N2. Col. 1: line, col. 2: wavelength, cols. 3 and 4: observed intensities relative to $H\beta$. The $H\beta$ flux is equal to 1.1 and 0.6×10^{-14} erg s $^{-1}$ cm $^{-2}$ in the AAT and WHT spectra respectively. An "h" in column 3 means that the line is outside the observed spectral range.

Line	λ (Å)	AAT	WHT
$H\beta$	4861.30	1.00	1.00
$H\alpha$	6562.80	3.36	3.38
[O III]	4958.90	3.40	3.40
[O III]	5006.80	10.30	10.30
[Ne III] 1F	3868.74	h	5.29
[Ne III] 1F	3967.51	h	1.68
[N II]	6548.10	1.14	1.15
[N II]	6583.40	3.37	3.40

2.3.3. The low-excitation narrow line system N3

The redshift of this system is $z=0.0610 \pm 0.0001$, very near the systemic redshift of the galaxy as determined from HI measurements. Its measured FWHM, corrected for the instrumental broadening, is 280 km s $^{-1}$ in agreement with Van Groningen (1993) who found 300 km s $^{-1}$. We found, in addition to the Balmer lines, [N II] λ 5755,6548,6583, [S II] λ 6716,6731, [S II] λ 4069,4076, [O I] λ 5577,6300,6363 and [Ca II] λ 7291,7324 (as well as Si II, NI and NII lines). These lines have previously been observed by Phillips (1976), Oke & Lauer (1979) or Osterbrock et al. (1990). Phillips (1976) found the [O II] lines to be too weak on their spectrum to be detected; Oke & Lauer (1979) found them to be present; another identification is possible for this feature, a Fe II (192) line at λ 3727.04. The theoretical ratio of the [S II] lines I(λ 4076)/I(λ 4069) is equal to 0.28, almost independent of temperature and density (Malkan

1983); in our model we set this ratio to the theoretical value.

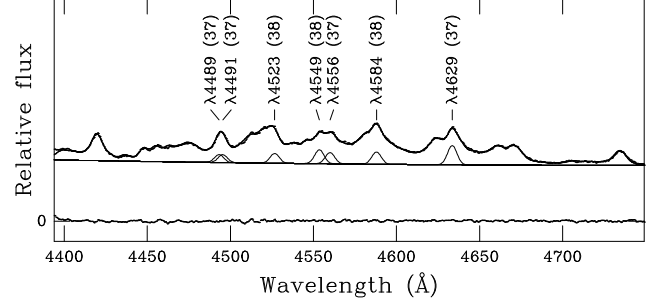


Fig. 4. The WHT blue spectrum in the range $\lambda\lambda$ 4394-4750 Å with the best fit and the residuals. Also shown are the seven strongest narrow permitted Fe II lines in this range, all belonging to multiplets 37 and 38.

In addition a number of both permitted and forbidden Fe II lines have been observed, as well as permitted Ni II, Ti II and Cr II lines. All lines used in the fit are listed in Table A.2. Fig. 4 shows a few of the observed narrow permitted Fe II lines in the spectral range $\lambda\lambda$ 4394-4750 Å in the WHT blue spectrum.

Table 5. Observed forbidden Fe II multiplets in the spectrum of I Zw 1 (in system N3). Col. 1: multiplet number, col. 2: transition, col. 3: upper level energy, col. 4: log N (see text).

m.	Transition	u.l.(eV)	log N
4F	a^6D-b^4P	2.78	0.30
6F	a^6D-b^4F	2.83	-0.27
7F	a^6D-a^6S	2.89	-0.07
14F	a^4F-a^2G	1.96	0.92
17F	a^4F-a^2D	2.64	0.27
18F	a^4F-b^4P	2.78	0.35
19F	a^4F-a^4H	2.67	0.00
20F	a^4F-b^4F	2.83	0.12
21F	a^4F-a^4G	3.21	-0.19
23F	a^4F-b^2H	3.34	0.24
34F	a^4D-b^2P	3.29	0.29
	a^2G-b^2D	4.49	-0.58

The observed [Fe II] multiplets are listed in Table 5. In any given multiplet, the intensity of each line has been forced to be proportional to its frequency and to the product R of its statistical weight $(2J+1)$ by its transition probability A taken from Quinet et al. (1996). Indeed, when the density is larger than the critical density ($\sim 10^4$ cm $^{-3}$) which is likely to be true here, the peak intensity of a line is $I \propto N \times R \times (\lambda/\lambda_0)^{-2}$ where N is the number of Fe $^{+}$ ions in the relevant state. In a collisionally excited cloud, $\log N = -5.040 \times (E/T) + k$, where E is the upper excitation potential in volts

and T the excitation temperature. We therefore have: $\log N = \log[I/R \times (\lambda/\lambda_o)^2] = -5.040 \times (E/T) + k$ (Thackeray 1967; Pagel 1969). We give in column 4 of Table 5 the measured quantity $\log N = \log[I/R \times (\lambda/5000)^2]$. These data are compatible with $T \sim 13\,000 \pm 3\,000$ K.

[Fe II] lines have previously been observed in the spectra of Seyfert 1 galaxies: IZw 1 (Oke & Lauer 1979), NGC 4151 (Netzer 1974) and HS 0328+05 (Véron et al. 2002). In IZw 1 Van Groningen (1993) observed an emission feature at ~ 5160 Å (for $z=0.061$) which he suggested could be either [Fe VI] $\lambda 5177$ at $z=0.057$ or [Fe VII] $\lambda 5158$ at $z=0.061$; this line in fact could rather be [Fe II] $\lambda 5159$.

2.4. Comparison of the WHT and AAT spectra

In the broad line system L1, the mean AAT to WHT line flux ratio is 2.10. In the narrow line system N3, it is 2.14. The line fluxes in the narrow line system are not expected to be variable, therefore the ratio of more than two observed between the AAT and WHT spectra should be due to a calibration error (differences in seeing, transparency, ?). The blue and red WHT spectra were obtained on October 1, 1998 and December 16, 1998 respectively, *i.e.* two months apart. The AAT spectrum was obtained on August 2, 1997, about 15 months earlier. The broad line intensities could have changed within 15 months. It does not however appear to be the case as the observed change is the same as for the narrow lines. The continuum of the AAT spectrum is 2.08 and 2.73 times stronger than the WHT blue and red continua respectively.

2.5. Discussion

2.5.1. The broad line region

Broad NaID emission ($\lambda\lambda 5890, 5896$) has been detected in the spectrum of IZw 1 (Phillips 1976). Oke & Lauer (1979) and Boroson & Meyers (1992) have measured $NaI/H\alpha = 0.019$ and 0.022 respectively; we found 0.043 . Only high-density models ($N_e \sim 10^{11} \text{ cm}^{-3}$) can produce such a large ratio, and only at column densities $N_H > 10^{23.5} \text{ cm}^{-2}$ (Kallman et al. 1987; Thompson 1991).

Ward et al. (1984) remarked that NaID is also seen in emission in novae, T Tauri stars and Me dwarfs; all these objects show strong Fe II emission suggesting that the excitation of NaID is related to the presence of or conditions causing the optical Fe II lines.

The Ca II infrared triplet lines ($\lambda\lambda 8498, 8542, 8662$) is strong in IZw 1 (Persson & McGregor 1985; van Groningen 1993). Emission in the Ca II triplet has been detected in a number of AGNs; the Ca II line strengths are roughly correlated with the strength of the optical Fe II emission. The Ca II line width is correlated with that of the O I $\lambda 8446$ line indicating that the gas that emit the Ca II lines is basically the same as that responsible for

Fe II emission (Persson 1988). Very large column densities are required to reproduce the Ca II spectrum (Ferland & Persson 1989); computed intensities of the Ca II triplet are in good agreement with observations if the emitting gas has a low temperature ($T < 8\,000$ K), a high density ($N_e > 10^{12} \text{ cm}^{-3}$) and a high column density ($N_H > 10^{23} \text{ cm}^{-2}$) (Joly 1989).

The weakness of C III] $\lambda 1909$ also indicates that $N_e \sim 10^{11} \text{ cm}^{-3}$ (Laor et al. 1997).

There is no strong evidence that the broad iron emission in IZw 1 is unusual compared with that of the average Seyfert 1 (Vestergaard & Wills 2001).

Joly (1987) has computed purely collisional models showing that low temperature ($T < 8\,000$ K), high density ($N_e > 10^{11} \text{ cm}^{-3}$), high column density ($N_H > 10^{22} \text{ cm}^{-2}$) clouds provide $Fe II_{opt}/H\beta$ in good agreement with observations of Seyfert 1 galaxies.

Observing evidences are accumulating showing that another process is also at work in the broad AGN emission line regions, namely the Ly α fluorescence, as first suggested by Penston (1987).

The UV spectrum of the QSO 2226–3905 is dominated by extremely strong Fe II_{UV} emission; the observed transitions are those predicted by the Ly α fluorescence models (Graham et al. 1996).

Fe II lines have been observed in emission in the near IR ($\lambda 9130, \lambda 9177$ and $\lambda 9203$) in several NLS1s (Rodríguez-Ardila et al. 2002). These lines are most likely due to the Ly α fluorescence mechanism (Rodríguez-Ardila et al. 2002; Sigut & Pradhan 2003).

The strongest Fe II emission features in the 0.8–2.5 μm spectral region in IZw 1 are the lines at $\lambda\lambda 9997, 10501, 10863$ and 11126 Å (the so-called “1 μm Fe II lines”) (Rudy et al. 2000). A combination of Ly α fluorescence and collisional excitation is found to be the main contributor (Rodríguez-Ardila et al. 2002; Sigut & Pradhan 2003).

Persson & McGregor (1985) have observed the O I $\lambda 8446$ line with a FWHM of $1\,400 \pm 200 \text{ km s}^{-1}$ in the spectrum of IZw 1. From the ratio $O I \lambda 11287 / \lambda 8446 = 0.76$ (Rudy et al. 2000), Rodríguez-Ardila et al. (2002) suggested that the broad O I lines in this object arise through both fluorescent excitation by Lyman α and collisional excitation.

As we have seen above, we have observed in the IZw 1 broad line region seven Fe II lines coming from a level at 13.25 eV above ground level. The likely presence of Fe II emission well below 2000 Å, and possibly even at ~ 1110 – 1130 Å, also indicates that Fe II is excited by processes other than just collisions, as the electron temperature in the Fe II region is most likely far too low for significant excitation of levels > 10 eV above the ground state (Laor et al. 1997).

The importance of Ly α pumping depends on the intrinsic width of this line, the excitation temperature

or source function of $\text{Ly}\alpha$ and the number of excited Fe^+ levels energetically accessible. This process can be very efficient; the most important conditions for efficient $\text{Ly}\alpha$ pumping is that the $\text{Ly}\alpha$ width be large enough for its profile to overlap the line profile of FeII transitions that originate from levels having a sufficiently low excitation energy to be thermally populated (Verner et al. 1999; Hartmann & Johansson 2000). If $\text{Ly}\alpha$ pumping is responsible for the population of levels at energies as high as 13.25 eV, levels around 3 eV have to be strongly populated via collisional processes which again imply high densities (Joly 1987).

From all these considerations one can infer that the density and column density in region L1 are very high and it is therefore necessary to take into account collisional excitation as well as continuum and Ly α fluorescence.

From the above discussion we can define reasonable initial parameters for modelling the BLR region of IZw 1. We estimated the dimension of the BLR using the relation between the BLR size and the luminosity of the central source deduced by Kaspi et al. (2000) from a reverberation mapping statistical study. Assuming an optical luminosity $\sim 3 \times 10^{44}$ erg s $^{-1}$ we infer a distance of the emission region $\sim 2 \times 10^{17}$ cm.

We have calculated a number of non-LTE models with the photoionization code CLOUDY with its large Fe $^{+}$ atom which includes 371 levels (Ferland 2002). The code takes into account collisional excitation as well as Ly α pumping (Ferland 2002; Verner et al. 1999). The Fe II predicted lines are gathered in a number of wavelength bands directly comparable to observations. The best fit with observations was obtained with our model 1 which has a density of 10^{12} cm $^{-3}$, a column density of 2.6×10^{23} cm $^{-2}$, an ionization parameter $U = 3 \times 10^{-3}$ and an overabundance of iron by a factor 3. The results are given in Table 6 where the first column lists the name of the line or the central wavelength of the Fe II band, the second column indicates the wavelength bounds of the band, columns 3 and 4 give the dereddened (using $E(B-V) = 0.20$) intensity ratios relative to H β measured respectively on the AAT and WHT spectra, and the last column gives the theoretical line ratios obtained from this model.

Unfortunately CLOUDY does not provide information on optical Si II and Ti II (nor on Cr II, Ni I, Ni II and [Ca II] observed in the NLR).

We also tried other models with U varying from 10^{-5} to 1 and density in the range 10^{10} - 10^{14} cm $^{-3}$. No photoionization model could produce strong enough Fe II emission. Whatever the gas density, Fe II strength saturates at large column density (10^{24} cm $^{-2}$). Moreover all these models, like model 1, predict He I and He II line intensities much stronger than observed. In the same way, although Ly α , C II, C IV, Mg II and the Balmer continuum are not in the presently observed wavelength range, we know that these features are weak in IZw 1 (Wu et al. 1980; Edelson & Malkan 1986; Laor et al. 1997) while they are very strong in all models.

To solve these problems it could be necessary to increase the emissivity of the excited H I region with respect to the H II region which could perhaps be obtained by an additional mechanical heating as proposed by Collin-Souffrin (1986).

Note however that the results of the models should be taken with caution as CLOUDY is used here with a range of parameters for which it is not adapted (namely a high column density, corresponding to a high optical thickness in the Balmer continuum, in the range $\tau = 0.1$ to 1.0) a condition where the escape probability approxima-

Table 6. Observed (dereddened) and computed line ratios referred to H β in system L1. Col. 1: line, col. 2: wavelength, cols. 3 and 4: observed intensities relative to H β , col. 5: computed intensity. An "h" in column 3 means that the line is outside the observed spectral range.

Line	$\lambda\lambda$ (Å)	AAT	WHT	model 1
H α		2.51	3.70	3.48
H γ		0.42	0.42	0.52
H δ		h	0.22	0.40
He I		h	0.13	0.34
He I	3705	h	0.05	-
He I	4026	h	0.08	0.38
He I	5876	0.08	0.11	2.39
He I	6678	0.04	0.07	0.54
He I	7065	0.02	0.05	1.95
He II	4686	0.00	0.00	0.80
Na I D	5890+5896	0.11	0.15	0.18
Fe II				
3590	3400-3780	h	0.80	0.52
3910	3780-4040	h	0.00	0.54
4060	4040-4080	h	0.00	0.01
4255	4080-4430	0.66	0.83	0.69
4558	4430-4685	1.46	1.86	0.81
4743	4685-4800	0.10	0.08	0.05
4855	4800-4910	0.08	0.04	0.15
4975	4910-5040	0.36	0.47	0.27
5070	5040-5100	0.00	0.00	0.03
5143	5100-5185	0.34	0.42	0.29
5318	5185-5450	1.14	1.39	0.57
5540	5450-5630	0.19	0.22	0.13
5865	5630-6100	0.07	0.11	0.18
6265	6100-6430	0.55	0.70	0.24
6565	6430-6700	0.46	0.73	0.19
6910	6700-7120	0.07	0.11	0.02

tion used in CLOUDY may be wrong (Collin-Souffrin & Dumont, 1986).

2.6. The low-excitation narrow line system

Oke & Lauer (1979) have found for the [N II] lines in this system $0.025 < I(\lambda 5755)/I(\lambda 6548 + \lambda 6583) < 0.2$. We measured 0.16. Assuming $T = 8000$ K, this corresponds to $N_e = 5 \times 10^5$ cm $^{-3}$ (Osterbrock 1974; Hamann 1994). The [S II] $I(\lambda 4069 + \lambda 4076)/I(\lambda 6716 + \lambda 6731)$ ratio appears to be significantly greater than one (Phillips 1976); we found ~ 4.5 . This observation suggests an electron density $N_e \sim 10^5$ cm $^{-3}$ (Hamann 1994). On the AAT spectrum, we found for the [O I] line ratio $I(\lambda 5777)/I(\lambda 6300 + \lambda 6363) \sim 0.3$ which, for $T = 8000$ K, implies $N_e \sim 10^7$ cm $^{-3}$ (Hamann 1994).

To explain the absence or weakness of lines like [O III] $\lambda 5007$ and [S II] $\lambda\lambda 6716, 6731$ and the prominence of lines with high critical densities, *i.e.* [O I] $\lambda 6300$, [N II] $\lambda 5755$, [S II] $\lambda\lambda 4069, 4076$, [Ca II] $\lambda\lambda 7291, 7324$ and [Ni II] $\lambda 7378, 7412$ in system N3, van Groningen (1993) argued that relatively high densities ($N_e > 10^{6-7}$ cm $^{-3}$)

are required. In addition the weakness or absence of [O II] λ 7324 and the strength of the [Ca II] $\lambda\lambda$ 7291,7324 lines which we observed show that it is a very low-ionization emission region and that most of the oxygen is probably in the atomic form O^o (Osterbrock et al. 1990).

Verner et al. (2000) have shown that, at low densities ($N_e < 10^2$ - 10^4 cm⁻³), the permitted optical Fe II lines are relatively weak, the reason being that the 63 lowest levels, the most populated at these densities, are all of the same (even) parity and are able to radiate only forbidden lines; the situation dramatically changes near density 10^6 cm⁻³ because, then, levels of odd parity are populated by collisions, enough to produce the permitted lines. If both the narrow permitted and forbidden Fe II lines are produced in the same region, the density should be larger than 10^6 cm⁻³ but lower than 10^8 cm⁻³ where forbidden lines are collisionally deexcited.

Non collisional excitation mechanisms, including pumping of high Fe II levels by the UV continuum and subsequent downward cascades, can also contribute significantly to the observed intensities of the optical [Fe II] lines (Verner et al. 2000).

In order to account for a very low ionization region such as N3 with the simultaneous presence of both Fe II and [Fe II], we computed models, using CLOUDY, in the range of density 10^5 to 10^8 cm⁻³ with a low ionization parameter.

Tables 7 and 8 give the two models which best encompass the observed line ratios. Model 1 has $N_e = 10^6$ cm⁻³ and $U = 10^{-6}$ while model 2 has $N_e = 10^7$ cm⁻³ and $U = 10^{-5}$. A region with "intermediate" characteristics ($10^6 < N_e < 10^7$ cm⁻³ and $10^{-6} < U < 10^{-5}$) might well represent the N3 system, in particular the [Fe II] and Fe II emissions. However some important discrepancies remain. The predicted [O I] intensity is much stronger than observed; the predicted He I λ 5876 relative intensity is 0.20 but this line is not observed.

As for the BLR, the discrepancy on He I might be weakened by a small enhancement of the temperature of the excited H I zone thanks to some additional mechanical heating. An increase of the electron density of the excited H I region would decrease the intensity of the [O I] lines.

In conclusion, this region is quite unusual in having a very low-excitation and being dominated by permitted and forbidden Fe II lines. To the best of our knowledge, no such emission region has ever been observed in any other AGN. But IZw 1 is lacking the usual high-excitation region always present in Seyfert galaxies at or near the systemic velocity. Regions N1 and N2 have a large blueshift.

An apparently very different astrophysical object, η Carinae, emits a very similar spectrum characterized by strong Fe II emission of both Fe II and [Fe II] lines (Zethson

Table 7. Observed and computed line ratios referred to H β in system N3. Col. 1: line, col. 2: wavelength, cols. 3 and 4: observed intensities relative to H β ; $F(H\beta) = 3.2 \times 10^{-14}$ and 3.3×10^{-14} erg cm⁻² s⁻¹ for the WHT and AAT spectra respectively (the Fe II band intensities include only the permitted lines), col. 5 and 6: computed line ratio relative to H β in models 1 and 2 (see text). An "h" in column 3 means that the line is outside the observed spectral range.

Line	$\lambda\lambda$	AAT	WHT	model 1	model 2
H α		5.06	2.16	2.87	2.76
H γ		0.40	0.36	0.47	0.47
H δ		h	0.17	0.27	0.27
H ϵ		h	0.10	0.17	0.16
He I	4026	h	0.00	0.03	0.03
He I	5876	0.00	0.00	0.20	0.2
[O I]	5577	0.10	0.00	0.08	0.0
[O I]	6300+6363	0.31	0.14	2.0	2.0
[O II]	3727	h	0.00	0.0	0.01
[O III]	4959+5007	0.00	0.00	0.0	0.0
[S II]	4069+4076	h	0.27	0.53	0.89
[S II]	6716+6731	0.21	0.06	0.19	0.04
[N II]	5755	0.24	0.08	0.01	0.08
[N II]	6548+6583	1.72	0.45	0.24	0.09
Fe II					
3590	3400-3780	h	0.59	0.05	0.33
3910	3780-4040	h	1.92	0.0	0.01
4060	4040-4080	h	0.00	0.0	0.0
4255	4080-4430	5.62	3.19	0.82	3.1
4558	4430-4685	5.76	3.14	0.30	0.87
4743	4685-4800	0.78	0.36	0.14	0.44
4855	4800-4910	0.66	0.12	0.36	1.02
4975	4910-5040	1.97	1.08	0.25	0.69
5070	5040-5100	0.00	0.00	0.04	0.09
5143	5100-5185	1.03	0.51	0.62	1.58
5318	5185-5450	3.80	2.24	1.18	2.98
5540	5450-5630	0.59	0.21	0.11	0.34
5865	5630-6100	0.78	0.37	0.03	0.12
6265	6100-6430	0.78	0.38	0.0	0.01
6565	6430-6700	0.77	0.40	0.05	0.06
6910	6700-7120	0.00	0.02	0.05	0.11

2001). η Carinae has been resolved into four components within 0''.3. The brightest component A is the central star; the other objects B, C and D are slow-moving ejecta with extremely unusual emission-line spectra. The central star is thought to be a massive star in an advanced stage of its evolution. Its UV spectrum do not correspond to any normal spectral type but suggests a composite of features seen in B-type supergiants in the range B2 Ia to B8 Ia (Ebbetts et al. 1997). Its mass has been estimated to be $\sim 70 M_\odot$, its luminosity $\sim 5 \times 10^6 L_\odot$ and its effective temperature $\sim 15\,000$ K (Hillier et al. 2001). Observations of the BD blobs show that the spectrum exhibits only low-ionization species; it displays no line of high ionization like [Ar III], [S III], [Fe III], [Fe IV] and [Ne III]. There is no [O II] emission. The [O I] line at λ 6300 is very weak. Narrow and

Table 8. Observed and computed [FeII] line ratios referred to H β in system N3. Col. 1: line, col. 2: wavelength, cols. 3 and 4: observed intensities relative to H β , cols. 5 and 6: computed intensities relative to H β . An "h" in column 3 or 4 means that the line is outside the observed spectral range.

lines	λ	AAT	WHT	model 1	model 2
4F	4728	0.14	0.09	0.09	0.29
4F	4890	0.15	0.10	0.16	0.49
6F	4416	0.52	0.31	0.14	0.41
6F	4458	0.26	0.15	0.08	0.22
6F	4493	0.07	0.04	0.02	0.05
7F	4359	0.38	0.16	0.08	0.22
7F	4414	0.27	0.11	0.05	0.15
7F	4475	0.08	0.03	0.02	0.05
14F	7155	0.27	h	0.66	0.80
14F	7172	0.08	h	0.28	0.27
17F	5527	0.13	0.06	0.03	0.11
18F	5273	0.22	0.14	0.21	0.56
18F	5433	0.07	0.04	0.06	0.17
19F	5112	0.07	0.04	0.08	0.19
19F	5159	0.36	0.19	0.42	0.98
19F	5220	0.06	0.03	0.07	0.17
19F	5262	0.22	0.11	0.26	0.61
19F	5297	0.04	0.02	0.05	0.11
19F	5334	0.14	0.08	0.18	0.42
19F	5376	0.12	0.06	0.14	0.34
20F	4775	0.15	0.04	0.04	0.12
20F	4815	0.59	0.16	0.14	0.41
20F	4905	0.22	0.06	0.07	0.20
20F	4947	0.08	0.02	0.02	0.06
20F	4951	0.10	0.03	0.04	0.10
20F	4973	0.12	0.03	0.04	0.11
21F	4177	0.07	0.03	0.02	0.08
21F	4244	0.49	0.23	0.10	0.48
21F	4245	0.10	0.05	0.02	0.11
21F	4277	0.29	0.14	0.07	0.31
21F	4306	0.08	0.04	0.02	0.09
21F	4320	0.19	0.09	0.04	0.20
21F	4347	0.11	0.05	0.02	0.10
21F	4353	0.13	0.06	0.03	0.14
21F	4358	0.18	0.09	0.04	0.20
21F	4372	0.09	0.05	0.02	0.10
23F	4114	h	0.05	0.02	0.07
23F	4179	0.00	0.01	0.00	0.01

strong Fe II and [FeII] emission lines are present. There is no Fe I or Fe III emission in the spectrum; the iron must therefore be almost entirely in the form of Fe⁺ (Zethson 2001; Verner et al. 2002).

The similarity between the spectra of region N3 in IZw 1 and of η Car is striking. Both are very low ionization clouds and both are dominated by permitted and forbidden Fe II emission lines. Fig. 5 shows a plot of the Fe II line relative intensities in region N3 *vs* their intensities in η Car. These intensities show some correlations: lines which are strong in one object tend to be strong in the other. The main difference is that the forbidden lines

are stronger in η Car and the permitted lines stronger in IZw 1 which could be due to a larger density in the last object.

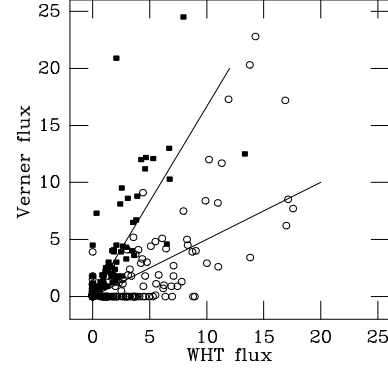


Fig. 5. Verner fluxes in η Carinae *vs* WHT fluxes in IZw 1 for the iron emission lines in system N3. The open circles represent the permitted lines, the filled squares the forbidden lines. This figure clearly shows that in IZw 1, the forbidden lines are about three to four times stronger with respect to the permitted lines than in η Carinae.

SS 7311 is another example of a nebula having a spectrum dominated by both permitted and forbidden Fe II lines, like η Carinae (Landaberry et al. 2001).

3. The Fe II template

Borson & Green (1992) have constructed a Fe II template by removing the lines identified as not being Fe II from the spectrum of IZw 1. The lines removed were the Balmer lines, the [O III] lines, [N II] λ 5755, a blend of Na I D and He I λ 5876 and two [Fe II] lines at λ 5158 and λ 5273.

We constructed a synthetic Fe II template in the wavelength range $\lambda\lambda$ 3535-7530 by using all the broad Fe II lines in system L1 as listed in Table A.1, giving them the intensity measured either on the AAT or the WHT spectra (for the lines measured on both the AAT and WHT spectra, we used the mean fluxes). The AAT line fluxes were divided by 2.1 in compliance with the result of our comparison of the WHT and AAT spectra (see sect. 2.4). The lines were given a Lorentzian profile with a FWHM=1 100 km s⁻¹.

The synthetic Fe II spectrum, corrected for internal extinction with a Galactic extinction law (Savage & Mathis 1979) and E(B-V)=0.20, can be used as a template, after a smoothing and a scaling suitable for each object. It is available in electronic form as an ASCII file with a step of one Å at <http://www.edpsciences.org>.

This synthetic spectrum differs from the Borson & Green's template mainly by the fact that we have identified a region (N3) dominated by narrow permitted and forbidden Fe II lines which are excluded from our template. The fluxes in these narrow lines are not negligible

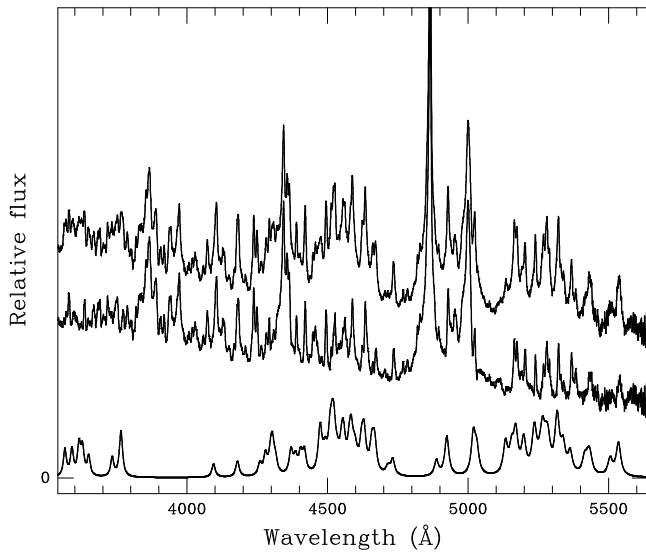


Fig. 6. This figure shows the blue deredshifted WHT spectrum of IZw 1 (top), the synthetic broad line Fe II spectrum built as explained in the text, uncorrected for reddening (bottom) and the difference (middle), shifted downward for clarity.

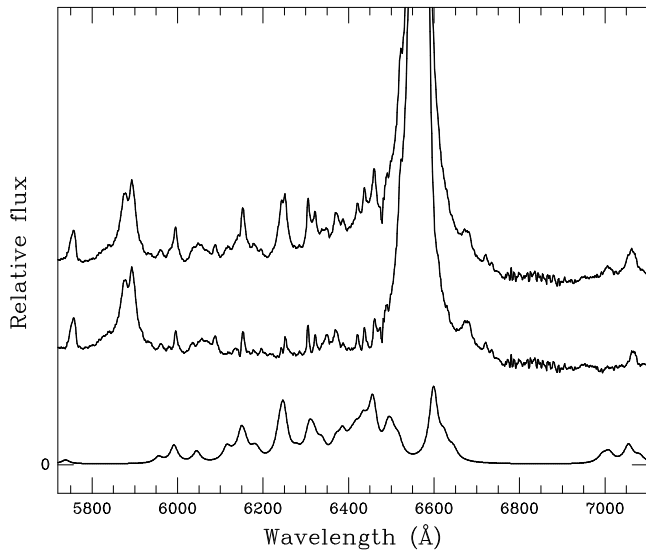


Fig. 7. This figure shows the red deredshifted WHT spectrum of IZw 1 (top), the synthetic broad line Fe II spectrum, uncorrected for reddening (bottom) and the difference (middle), shifted downward for clarity.

compared to the fluxes in the broad Fe II lines and consequently our template may differ significantly from the Boroson & Green template (see Figs. 6 and 7).

The Boroson & Green template has relatively weak lines near 6400-6500 Å; the H α line in IZw 1 has a blue wing which does not exist in the H β line; therefore this wing is not due to H α emission and is, at least partially, due to a blend of Fe II lines.

4. Conclusion

The analysis of very high signal-to-noise, intermediate resolution spectra of IZw 1 has confirmed the complexity of the emission line spectrum of this object. The major result is that the main narrow line system is quite unlike those observed in the majority of Seyfert galaxies. The density is relatively large: $10^6 < N_e < 10^7 \text{ cm}^{-3}$. The excitation is very low. The spectrum is dominated by both permitted and forbidden Fe II lines. This spectrum is very similar to that of the blobs of the Galactic nebula η Car.

We did not succeed in modelling the spectrum of the broad-line region and we suggest that a non radiative heating mechanism increases the temperature in the high density ($\sim 10^{11} \text{ cm}^{-3}$) excited H I region, thus providing the necessary additional excitation of the Fe II lines. We found that this region is not atypical. But the fact that these lines are quite narrow together with the use of very high signal-to-noise spectra allowed us to detect with some reliability a number of high-excitation Fe II lines not previously observed in Seyfert 1 nuclei.

We have used these data to build a template spectrum of the broad Fe II emission.

5. Acknowledgments

We gratefully thank S. Collin-Souffrin for helpful discussions and Prof. S. Johansson for providing us with a copy of Dr. T. Zethson's thesis.

References

- Boroson T.A. & Green R.F. 1992, ApJS 80,109
- Boroson T.A. & Meyers K.A. 1992, ApJ 397,442
- Collin-Souffrin S. 1986, A&A 166,115
- Collin-Souffrin S. & Dumont S. 1986, A&A 166,13
- Collin-Souffrin S., Dumont S. & Tully M. 1982, A&A 106,362
- Condon J.J., Hutchings J.B., Gower A.C. 1985, AJ 90,1642
- Ebbetts D.C., Walborn N.R. & Parker J.W. 1997, ApJ 489,L61
- Eckart A., van den Werf P.P., Hofmann R. & Harris A.I. 1994, ApJ 424,627
- Edelson R.A. & Malkan M.A. 1986, ApJ 308,59
- Ferland G.J., 2002, Hazy, a Brief Introduction to Cloudy, University of Kentucky, Department of Physics and Astronomy, Internal Report
- Ferland G.J. & Persson S.E. 1989, ApJ 347,656
- Galavis M.E., Mendoza C. & Zeppen C.J. 1997, A&AS 123,159
- Giannuzzo M.E., Mignoli M., Stirpe G.M. & Comastri A. 1998, A&A 330,894
- Goodrich R.W. 1990, ApJ 355,88
- Graham M.J., Clowes R.G. & Campusano L.E. 1996, MNRAS 279,1349
- Hamann F. 1994, ApJS 93,485
- Hartmann H. & Johansson S. 2000, A&A 359,627
- Hillier D.J., Davidson K., Ishibashi K. & Gull T. 2001, ApJS 552,837
- Hirata R. & Horaguchi T. 1995, <http://amods.kaeri.re.kr/>

- Holt J., Tadhunter C.N., Morganti R. 2003, MNRAS 342,227
- Joly M. 1987, A&A 184,33
- Joly M. 1988, A&A 192,87
- Joly M. 1989, A&A 208,47
- Kallman T., Lepp S. & Giovannini P. 1987, ApJ 321,907
- Kaspi S., Smith P.S., Netzer H. et al. 2000, ApJ 533,631
- Landaberry S.J.C., Pereira C.B. & Araujo F.X. de 2001, A&A 376,917
- Laor A., Januzzi B.T., Green R.F. & Boroson T.A. 1997, ApJ 489,656
- Malkan M.A. 1983, ApJ 264,L1
- Merrill P.W. 1951, ApJ 114,37
- Merrill P.W. 1961, ApJ 133,503
- Netzer H. 1974, MNRAS 169,579
- Neugebauer G., Oke J.B., Becklin E.E. & Matthews K. 1979, ApJ 230,79
- Oke J.B. & Lauer T.R. 1979, ApJ 230,360
- Osterbrock D.E. 1974, Astrophysics of gaseous nebulae, Freeman, San Francisco
- Osterbrock D.E., Koski A.T. & Phillips M.M. 1976, ApJ 206,898
- Osterbrock D.E., Shaw R.A. & Veilleux S. 1990, ApJ 352,561
- Pagel B.E.J. 1969, Nature 221,325
- Penston M.V. 1987, MNRAS 229,1P
- Persson S.E. 1988, ApJ 330,751
- Persson S.E. & McGregor P.J. 1985, ApJ 290,125
- Peterson B.M., Foltz C.B., Crenshaw D.M., Meyers K.A. & Byard P.L. 1984, ApJ 279,529
- Phillips M.M. 1976, ApJ 208,37
- Phillips M.M. 1978, ApJ 226,736
- Quinet P., Le Dourneuf M. & Zeippen C.J. 1996, A&AS 120,361
- Rafanelli P. 1985, A&A 146,17
- Rodríguez-Ardila A., Viegas S.M., Pastoriza M.G. & Prato L. 2002, ApJ 565,140
- Rudy R.J. & Willner S.P. 1983, ApJ 267,L69
- Rudy R.J., Mazuk S., Puetter R.C. & Hamann F. 2000, ApJ 539,166
- Sargent W.L.W. 1968, ApJ 152,L31
- Savage B.D. & Mathis J.S. 1979, ARA&A 17,73
- Schinnerer E., Eckart A. & Tacconi L.J. 1998, ApJ 500,147
- Schlegel D.J., Finkbeiner D.P. & Davis M. 1998, ApJ 500,525
- Sigut T.A.A. & Pradhan A.K. 2003, ApJS 145,15
- Smith J.E., Young S., Robinson A. et al. 2002, MNRAS 335,773
- Stark A.A., Gammie C.F., Wilson R.W. et al. 1992, ApJS 79,77
- Stone R.P.S. 1977, ApJ 218,767
- Tadhunter C., Wills K., Morganti R., Oosterloo T. & Dickson R. 2001, MNRAS 327,227
- Thackeray A.D. 1967, MNRAS 135,51
- Thompson K.L. 1991, ApJ 374,496
- Van Groningen E. 1993, A&A 272,25
- van Hoof P., <http://www.pa.uky.edu/~peter/atomic/>
- Verner E.M., Verner D.A., Korista K.T. et al. 1999, ApJS 120,101
- Verner E.M., Verner D.A., Baldwin J.A., Ferland G.J. & Martin P.G. 2000, ApJ 543,831
- Verner E.M., Gull T.R., Bruhweiler F. et al. 2002, ApJ 581,1154
- Véron P., Lindblad P.O., Zuiderwijk E.J., Véron-Cetty M.-P. & Adams G. 1980, A&A 87,245
- Véron P., Gonçalves A.C. & Véron-Cetty M.-P. 2002, A&A 384,826
- Vestergaard M. & Wilkes B.J. 2001, ApJS 134,1
- Ward M.J., Morris S.L. & Penston M.V. 1984, MNRAS 206,5P
- Wills B.J. 1983, in: Quasars and gravitational lenses, Lige, p. 458
- Winkler H. 1997, MNRAS 292,273
- Wu C.C., Boggess A. & Gull T.R. 1980, ApJ 242,14
- Zethson T. 2001, PhD thesis, Lund university
- Zwicky F. 1964, First list of compact galaxies, CIT, Pasadena
- Zwicky F. 1971, Catalogue of selected compact galaxies and of post-eruptive galaxies, CIT, Pasadena

Appendix A: Line lists for regions L1 and N3

Table A.1. List of all lines used in the fits of the broad system L1 of the AAT or WHT spectra. Col. 1: line, col. 2: transition, col. 3: upper level energy, col. 4: wavelength, cols. 5 and 6: observed intensities relative to $H\beta$, corrected for a reddening of $E(B-V)=0.2$. An "h" in column 5 or 6 means that the line is outside the observed spectral range while an "n" means that it has not been detected.

Line	Transition	ul(eV)	λ (Å)	AAT	WHT
$H\beta$		12.75	4861.30	1.00	1.00
$H\alpha$		12.09	6562.79	2.51	3.70
$H\gamma$		13.05	4340.40	0.42	0.42
$H\delta$		13.22	4101.73	h	0.22
$H\epsilon$		13.32	3970.07	h	0.13
H 8		13.39	3889.05	h	0.08
H 9		13.43	3835.38	h	0.06
H 10		13.46	3797.90	h	0.04
H 11		13.49	3770.63	h	0.03
H 12		13.50	3750.15	h	0.02
Fe II 113	c2G-z4Io	7.63	3564.53	h	0.11
Fe II	d2G-u2Fo	10.72	3589.48	h	0.11
Fe II]112	c2G-z4Ho	7.58	3614.87	h	0.12
Fe II 193	d2D1-w2Fo	9.37	3627.17	h	0.11
Fe II	w4Do-f4F	12.39	3649.39	h	0.08
He I 25	3Po-3D	24.31	3705.00	h	0.05
Fe II]	d4P-v2Do	10.46	3732.88	h	0.08
Ti II 72	b2D-y2Do	4.89	3741.63	h	0.07
Fe II 29	b4P-z4Po	5.88	3764.09	h	0.19
He I 18	3Po-3D	24.04	4026.36	h	0.08
Fe II	z4Go-e4G	10.60	4093.66	h	0.06
Fe II 28	b4P-z4Fo	5.55	4178.86	0.05	0.07
Fe II 28	b4P-z4Fo	5.62	4258.16	0.05	0.04
Fe II 32	a4H-z4Fo	5.59	4278.10	0.06	0.09
Fe II 28	b4P-z4Fo	5.59	4296.57	0.06	0.07
Fe II 27	b4P-z4Do	5.58	4303.17	0.10	0.12
Fe II 32	a4H-z4Fo	5.55	4314.29	0.05	0.05
Fe II 28	b4P-z4Fo	5.62	4369.40	0.07	0.12
Fe II 27	b4P-z4Do	5.60	4385.38	0.07	0.05
Fe II	y4Fo-e4G	10.52	4403.03	0.07	0.09
Fe II 27	b4P-z4Do	5.58	4416.82	0.08	0.09
Fe II 37	b4F-z4Fo	5.62	4472.92	0.15	0.21
Fe II 37	b4F-z4Fo	5.59	4489.18	0.04	0.04
Fe II 37	b4F-z4Fo	5.62	4491.40	0.04	0.04
Fe II 38	b4F-z4Do	5.60	4508.28	0.10	0.14
Fe II 37	b4F-z4Fo	5.59	4515.34	0.09	0.10
Fe II 37	b4F-z4Fo	5.55	4520.22	0.07	0.10
Fe II 38	b4F-z4Do	5.58	4522.63	0.07	0.10
Fe II 37	b4F-z4Fo	5.59	4534.17	0.02	0.07
Fe II 38	b4F-z4Do	5.55	4549.47	0.08	0.07
Fe II 37	b4F-z4Fo	5.55	4555.89	0.11	0.14
Ti II 50	a2P-z2Do	3.94	4563.76	0.08	0.14
Fe II 38	b4F-z4Do	5.55	4576.33	0.06	0.07
Fe II 37	b4F-z4Fo	5.55	4582.83	0.07	0.08
Fe II 38	b4F-z4Do	5.51	4583.83	0.07	0.08
Ti II 50	a2P-z2Do	3.94	4589.98	0.07	0.13
Fe II 38	b4F-z4Do	5.55	4595.68	0.06	0.07
Fe II] 43	a6S-z4Do	5.58	4601.41	0.01	0.04
Fe II 38	b4F-z4Do	5.51	4620.51	0.10	0.10
Fe II 37	b4F-z4Fo	5.48	4629.34	0.12	0.17
Fe II] 43	a6S-z4Do	5.55	4656.97	0.09	0.13
Fe II 37	b4F-z4Fo	5.48	4666.75	0.12	0.12
Fe II] 26	b4P-z6Po	5.41	4713.18	0.03	0.03
Fe II] 54	b2P-z4D0	5.82	4720.15	n	0.01

Table A.1. (continued)

Line	Transition	ul(eV)	λ (Å)	AAT	WHT
Fe II] 54	b2P-z4Po	5.88	4886.93	0.08	0.04
Fe II 42	a6S-z6Po	5.41	4923.92	0.14	0.18
Fe II 42	a6S-z6Po	5.36	5018.45	0.14	0.18
Fe II	e6F-4[5]	12.75	5030.64	0.08	0.11
Si II 5	2Po-2D	12.53	5041.06	0.03	0.05
Si II 5	2Po-2D	12.53	5056.35	0.03	0.03
Fe II] 35	b4F-z6Fo	5.22	5132.67	0.12	0.13
Fe II] 35	b4F-z6Fo	5.25	5154.40	0.08	0.11
Fe II 42	a6S-z6Po	5.29	5169.03	0.14	0.18
Ti II 70	b2D-z2Do	3.97	5188.68	0.06	0.06
Fe II 49	a4G-z4Fo	5.62	5197.57	0.11	0.15
Fe II 49	a4G-z4Fo	5.59	5234.62	0.13	0.15
Fe II 41	a6S-z6Fo	5.26	5238.58	0.03	0.05
Fe II 49	a4G-z4Fo	5.59	5254.92	0.02	0.01
Fe II 41	a6S-z6Fo	5.25	5256.89	0.02	0.01
Fe II 48	a4G-z4Do	5.58	5264.80	0.12	0.17
Fe II 49	a4G-z4Fo	5.55	5275.99	0.05	0.08
Fe II 41	a6S-z6Fo	5.24	5284.09	0.10	0.12
Fe II 49	a4G-z4Fo	5.48	5316.61	0.16	0.19
Fe II 48	a4G-z4Do	5.55	5316.78	0.05	0.06
Fe II 48	a4G-z4Do	5.55	5337.71	0.09	0.12
Fe II 48	a4G-z4Do	5.51	5362.86	0.08	0.08
Fe II 48	a4G-z4Do	5.51	5414.09	0.06	0.07
Fe II 49	a4G-z4Fo	5.48	5425.27	0.04	0.04
Fe II] 55	b2H-z4Fo	5.55	5432.98	0.06	0.09
Fe II	y4Do-e4D	9.90	5505.25	0.07	0.07
Fe II] 55	b2H-z4Fo	5.48	5534.83	0.12	0.15
Fe II	p6Po-4d4F	13.25	5738.18	n	0.01
Si II 8	4Po-4P	16.62	5827.80	0.02	0.02
Si II 8	4Po-4P	16.62	5846.12	0.01	0.02
Si II 8	4Po-4P	16.64	5868.40	0.04	0.05
He I 11	3Po-3D	23.07	5875.70	0.08	0.11
Na I D	2S-2Po	2.10	5889.89	0.04	0.04
Na I D	2S-2Po	2.10	5895.89	0.07	0.11
Fe II 217	x4Do-e4D	9.96	5955.51	0.01	0.02
Fe II] 46	a4G-z6Fo	5.22	5991.39	0.03	0.05
Fe II] 46	a4G-z6Fo	5.20	6044.53	0.02	0.03
Fe II] 46	a4G-z6Fo	5.25	6113.32	0.01	0.02
Fe II] 46	a4G-z6Fo	5.26	6116.04	0.01	0.02
Fe II] 46	a4G-z6Fo	5.22	6129.71	0.01	0.01
Fe II 74	b4D-z4Po	5.90	6147.74	0.03	0.03
Fe II 74	b4D-z4Po	5.90	6149.25	0.03	0.03
Fe II	p4So-4d4F	13.25	6157.12	0.02	0.04
Fe II] 46	a4G-z6Fo	5.25	6178.14	0.01	0.02
Fe II] 46	a4G-z6Fo	5.20	6185.34	0.02	0.02
Fe II 74	b4D-z4Po	5.88	6238.37	0.04	0.05
Fe II 74	b4D-z4Po	5.88	6247.55	0.10	0.13
Fe II	a2F-z6Po	5.36	6278.22	0.01	0.02
Fe II] 34	b4F-z6Do	4.79	6307.53	0.05	0.07
Fe II	z4Do-c4D	7.47	6317.99	0.04	0.05
Fe II	p4Fo-4d4F	13.25	6336.95	0.03	0.04
Si II 2	2S-2Po	10.07	6347.10	0.03	0.04
Fe II 40	a6S-z6Do	4.84	6369.45	0.03	0.04
Si II 2	2S-2Po	10.07	6371.40	0.02	0.03
Fe II	z4Do-c4D	7.49	6385.45	0.05	0.05
Fe II	z6Do-b4G	6.73	6402.90	0.01	0.02
Fe II 74	b4D-z4Po	5.82	6407.30	0.01	0.02
Fe II 74	b4D-z4Po	5.82	6416.89	0.03	0.05
Fe II 40	a6S-z6Do	4.82	6432.68	0.06	0.06
Fe II	z4Fo-c4D	7.47	6442.95	0.02	0.02
Fe II 74	b4D-z4Po	5.82	6456.20	0.11	0.14

Table A.1. (end)

Line	Transition	ul(eV)	λ (Å)	AAT	WHT
Fe II	z4Do-c4D	7.49	6491.28	0.04	0.07
Fe II]	x4Do-e6D	9.78	6500.63	0.03	0.06
Fe II 40	a6S-z6Do	4.79	6516.07	0.01	0.08
Fe II	z4Fo-c4D	7.49	6598.30	0.14	0.21
Fe II	z4Fo-c4D	7.49	6623.07	0.03	0.06
Fe II]	e6G-2Go	12.37	6644.25	0.02	0.03
He I 46	1Po-1D	23.07	6678.11	0.04	0.07
Fe II	v4Fo-4d4F	13.23	6993.43	0.02	0.01
Fe II	u2Go-4d4F	13.25	7008.69	0.02	0.03
Fe II	u2Do-4d4F	13.25	7054.53	0.04	0.05
He I 10	3Po-3S	22.72	7065.42	0.02	0.05
Fe II	u2Go-4d4F	13.23	7080.47	n	0.02
Fe II 73	b4D-z4Do	5.60	7224.51	0.04	h
Fe II 73	b4D-z4Do	5.58	7307.97	0.05	h
Fe II 73	b4D-z4Do	5.58	7320.70	0.06	h

Table A.2. List of all lines used in the fits of system N3 of the AAT or WHT spectra. Col. 1: line, col. 2: transition, col. 3: upper level energy, col. 4: wavelength, cols. 5 and 6: observed intensities relative to H β . An "h" in column 5 or 6 means that the line is outside the observed spectral range while an "n" means that it has not been detected.

Line	Transition	ul(eV)	λ (Å)	AAT	WHT
H α		12.09	6562.80	5.06	2.16
H β		12.75	4861.30	1.00	1.00
H γ		13.05	4340.40	0.40	0.36
H δ		13.22	4101.73	h	0.17
H ϵ		13.32	3970.07	h	0.10
H 8		13.39	3889.05	h	0.06
H 9		13.43	3835.38	h	0.04
H 10		13.46	3797.90	h	0.03
H 11		13.49	3770.63	h	0.02
H 12		13.50	3750.15	h	0.02
Fe II 113	c2G-z4Io	7.63	3564.54	h	0.04
Fe II]	c4F-v2Fo	9.69	3572.97	h	0.07
Ni II 4	4P-4Do	6.54	3576.76	h	0.15
Fe II	d2G-u2Fo	10.72	3589.48	h	0.04
Ti II 15	a2F-z4Do	4.05	3596.05	h	0.06
Cr II 13	a4P-z6Do	6.15	3603.61	h	0.05
Cr II 13	a4P-z6Do	6.12	3631.72	h	0.15
Cr II 1	a4P-z6Fo	5.86	3644.69	h	0.04
Cr II 156	b2I-z2Io	8.38	3650.37	h	0.02
Fe II]	c2G-z4Go	7.54	3661.17	h	0.08
Cr II 156	b2I-z2Io	8.37	3664.94	h	0.10
Cr II 12	a4P-z4Po	6.08	3677.93	h	0.14
Ti II 14	a2F-z2Do	3.94	3685.19	h	0.18
Fe II]	z2Do-4P	10.93	3693.93	h	0.02
Fe II]	b2D-x4Do	7.84	3699.90	h	0.02
Cr II 12	a4P-z4Po	6.04	3712.97	h	0.12
Cr II 20	b4D-z4Fo	6.44	3715.19	h	0.07
Fe II]	a2D2-z4Po	5.88	3720.17	h	0.06
Fe II]	y4Po-4P	10.93	3722.47	h	0.04
Fe II 192	d2D1-x2Do	9.24	3727.04	h	0.07
Cr II]	a4G-z6Fo	5.86	3742.99	h	0.08
Fe II 154	c2D-z2Po	8.04	3748.48	h	0.12
Fe II 29	b4P-z4Po	5.88	3764.09	h	<0.01
Cr II 20	b4D-z4Fo	6.40	3767.18	h	0.07
Fe II 192	d2D1-x2Do	9.24	3778.37	h	0.03
Fe II]	a2P-z4Do	5.55	3783.34	h	0.15
Ti II]	a2F-z4Fo	3.82	3814.58	h	0.16
Fe II]	a2P-z4Do	5.58	3821.92	h	0.13
Fe II 29	b4P-z4Po	5.82	3824.91	h	0.03
Fe II 153	c2D-z2Fo	7.97	3827.08	h	0.13
Fe II]	a2D2-z4Po	5.88	3833.01	h	0.05
Ni II 11	2G-2Fo	7.25	3849.58	h	0.15
Fe II 29	b4P-z4Po	5.90	3872.77	h	0.11
Fe II]	b2D-y6Po	7.69	3875.45	h	0.05
Fe II]	c4F-w2Fo	9.41	3879.02	h	0.19
Fe II]	w2Do-6F	12.95	3884.56	h	0.25
Ti II 34	a2G-z2Go	4.31	3900.55	h	0.10
Cr II 167	b2D-z2Fo	8.50	3905.64	h	0.06
Fe II]	a4P-z6Do	4.84	3914.48	h	0.15
Fe II]	a4P-z6Do	4.85	3930.31	h	0.13
Fe II]	c4F-w2Fo	9.37	3933.86	h	0.14
Fe II]	a4P-z6Do	4.82	3938.29	h	0.17
Fe II]	a4P-z6Do	4.84	3945.21	h	0.04
Fe II]	a4P-z6Do	4.85	3966.43	h	0.07
Fe II 29	b4P-z4Po	5.82	3974.16	h	0.06

Table A.2. (continued)

Line	Transition	ul(eV)	λ (Å)	AAT	WHT
Fe II] 3	a4P-z6Do	4.84	3981.61	h	0.06
Cr II 194	b2D-x4Do	8.41	4003.33	h	0.06
Ni II 12	a2G-z2D	7.12	4015.50	h	0.04
Fe II 126	b2D-z4G	7.56	4032.95	h	0.01
Ti II 87	b2G-y2Fo	4.95	4053.81	h	0.06
Cr II 19	b4D-z6Do	6.16	4063.94	h	0.06
[S II] 1F	4So-2Po	3.05	4068.62	h	0.21
[S II] 1F	4So-2Po	3.04	4076.22	h	0.06
[Fe II] 23F	a4F-b2H	3.24	4114.47	h	0.05
Fe II	z4Ho-e4G	10.56	4114.55	h	0.03
Fe II 28	b4P-z4Fo	5.59	4122.64	h	0.17
Fe II 27	b4P-z4Do	5.58	4128.73	h	0.16
[Fe II] 21F	a4F-a4G	3.22	4146.65	h	0.00
Ti II 105	b2F-x2Do	5.57	4163.64	0.13	0.04
Fe II]149	c2D-y4Fo	7.71	4167.69	n	0.03
Fe II 27	b4P-z4Do	5.68	4173.45	0.65	0.23
[Fe II] 21F	a4F-a4G	3.20	4177.21	0.07	0.03
Fe II] 21	a2D2-z4Do	5.51	4177.70	0.17	0.13
Fe II 28	b4P-z4Fo	5.55	4178.86	0.17	0.13
[Fe II] 23F	a4F-b2H	3.27	4178.96	n	0.01
Fe II] 21	a2D2-z4Do	5.60	4183.20	0.17	0.09
Fe II]	b4G-v2Fo	9.69	4190.96	0.09	0.05
Fe II]	z2Do-f4D	10.52	4204.48	0.02	0.05
Fe II] 45	a6S-z4Po	5.82	4227.17	0.32	0.12
[Fe II] 21F	a4F-a4G	3.23	4231.56	0.01	0.00
Fe II 27	b4P-z4Do	5.51	4233.17	0.76	0.40
Fe II]	z2Do-f4D	10.50	4237.57	0.21	0.11
[Fe II] 21F	a4F-a4G	3.15	4243.97	0.49	0.23
[Fe II] 21F	a4F-a4G	3.22	4244.81	0.10	0.05
Fe II	y4Po-f4D	10.52	4247.24	0.17	0.09
[Fe II] 23F	a4F-b2H	3.27	4251.44	n	0.01
Fe II 220	x4Do-e4F	10.71	4259.32	0.16	0.08
[Fe II] 21F	a4F-a4G	3.20	4276.83	0.29	0.14
[Fe II] 7F	a6D-a6S	2.89	4287.39	0.53	0.22
Fe II 28	b4P-z4Fo	5.59	4296.57	0.11	0.05
Fe II 27	b4P-z4Do	5.58	4303.17	0.16	0.08
[Fe II] 21F	a4F-a4G	3.23	4305.89	0.08	0.04
Fe II 32	a4H-z4F	5.55	4314.29	0.21	0.10
[Fe II] 21F	a4F-a4G	3.22	4319.62	0.19	0.09
Fe II 220	x4Do-e4F	10.71	4319.68	0.17	0.05
Fe II] 20	a2D2-z6Po	5.41	4327.04	0.41	0.10
Fe II] 202	c4F-w2Go	9.07	4346.51	n	0.04
[Fe II] 21F	a4F-a4G	3.15	4346.85	0.11	0.05
Fe II 27	b4P-z4Do	5.55	4351.76	0.84	0.40
[Fe II] 21F	a4F-a4G	3.20	4352.78	0.13	0.06
[Fe II] 21F	a4F-a4G	3.23	4358.36	0.18	0.09
Fe II] 202	c4F-w2Go	9.06	4359.12	0.36	0.21
[Fe II] 7F	a6D-a6S	2.89	4359.34	0.38	0.16
[Fe II] 21F	a4F-a4G	3.22	4372.43	0.09	0.05
[Fe II] 6F	a6D-b4F	2.83	4382.74	0.05	0.03
Fe II 27	b4P-z4Do	5.60	4385.38	0.49	0.26
Ti II 19	a2D-z2Fo	3.90	4395.03	0.13	0.08
[Fe II] 7F	a6D-a6S	2.89	4413.78	0.27	0.11
[Fe II] 6F	a6D-b4F	2.81	4416.27	0.52	0.31
Ti II 93	b2P-y2Do	4.91	4421.95	0.14	0.07
[Fe II] 6F	a6D-b4F	2.84	4432.45	0.04	0.02
Fe II]	y4Fo-e6G	10.50	4432.84	0.06	0.05
Fe II 222	y4Go-e4F	10.74	4440.76	n	0.04
Ti II 19	a2D-z2Fo	3.87	4443.80	0.43	0.20

Table A.2. (continued)

Line	Transition	ul(eV)	λ (Å)	AAT	WHT
Ti II 19	a2D-z2Fo	3.87	4450.49	0.11	0.09
Fe II	a2F-c4F	6.21	4452.01	0.11	0.10
[Fe II] 7F	a6D-a6S	2.89	4452.11	0.17	0.07
[Fe II] 6F	a6D-b4F	2.83	4457.94	0.26	0.15
Ti II] 40	a4P-z2Do	3.94	4464.46	0.14	0.07
[Fe II] 7F	a6D-a6S	2.89	4474.90	0.08	0.03
[Fe II] 6F	a6D-b4F	2.84	4488.75	0.10	0.06
Fe II 37	b4F-z4Fo	5.59	4489.18	0.27	0.17
Fe II 37	b4F-z4Fo	5.62	4491.40	0.27	0.17
[Fe II] 6F	a6D-b4F	2.81	4492.63	0.07	0.04
Fe II 38	b4F-z4Do	5.60	4508.28	0.17	0.09
Fe II 37	b4F-z4Fo	5.59	4515.34	0.23	0.12
Fe II 37	b4F-z4Fo	5.55	4520.22	0.27	0.14
Fe II 38	b4F-z4Do	5.58	4522.63	0.38	0.19
[Fe II] 6F	a6D-b4F	2.84	4528.38	0.03	0.02
Fe II 37	b4F-z4Fo	5.59	4534.17	0.34	0.12
Fe II 38	b4F-z4Do	5.58	4541.52	0.34	0.16
Fe II 38	b4F-z4Do	5.55	4549.47	0.37	0.19
Fe II 37	b4F-z4Fo	5.55	4555.89	0.28	0.14
Fe II 38	b4F-z4Do	5.55	4576.34	0.21	0.11
Fe II 37	b4F-z4Fo	5.55	4582.83	0.05	0.02
Fe II 38	b4F-z4Do	5.51	4583.83	0.48	0.26
Cr II 44	b4F-z4Do	6.76	4616.64	0.15	0.08
Fe II 38	b4F-z4Do	5.51	4620.51	0.29	0.14
Fe II 37	b4F-z4Fo	5.48	4629.34	0.80	0.41
Fe II 25	b4P-z6F	5.26	4634.60	0.32	0.21
[Fe II] 4F	a6D-b4P	2.78	4639.67	0.07	0.05
N II 5	3Po-3P	21.15	4643.09	0.25	0.07
Fe II] 43	a6S-z4Do	5.55	4656.97	0.17	0.08
[Fe II] 4F	a6D-b4P	2.78	4664.44	0.02	0.02
Fe II 37	b4F-z4Fo	5.48	4666.75	0.14	0.13
Fe II 25	b4P-z6F	5.24	4670.17	0.17	0.08
Cr II	c2D-y4Fo	8.31	4697.60	0.07	0.03
Fe II	y6Po-e6F	10.33	4702.54	0.08	0.02
[Fe II] 4F	a6D-b4P	2.70	4728.07	0.14	0.09
Fe II] 43	a6S-z4Do	5.51	4731.44	0.25	0.18
Fe II 50	a4G-z4Po	5.82	4763.79	0.23	0.08
[Fe II] 20F	a4F-b4F	2.83	4774.72	0.15	0.04
Fe II 50	a4G-z4Po	5.82	4780.60	0.20	0.07
[Fe II] 4F	a6D-b4P	2.70	4798.27	0.02	0.01
Fe II]	b4D-z8Po	6.48	4802.61	0.34	0.05
[Fe II] 20F	a4F-b4F	2.81	4814.53	0.59	0.16
Cr II 30	a4F-z4Fo	6.44	4824.13	0.60	0.17
Cr II 30	a4F-z4Fo	6.42	4836.22	0.50	0.05
[Fe II] 20F	a4F-b4F	2.84	4874.48	0.15	0.04
Cr II 30	a4F-z4Fo	6.41	4876.48	0.18	0.09
[Fe II] 4F	a6D-b4P	2.58	4889.62	0.15	0.10
Fe II 36	b4F-f6Po	5.36	4893.83	0.31	0.07
[Fe II]	a2G-b2D	4.49	4898.61	0.09	0.05
[Fe II] 20F	a4F-b4F	2.83	4905.34	0.22	0.06
Ti II 114	c2D-y2Po	5.65	4911.20	0.28	0.06
Fe II 42	a6S-z6Po	5.41	4923.92	0.79	0.39
Fe II]	z2Fo-e6G	10.50	4928.31	0.17	0.09
N I 9	2P-2So	13.20	4935.03	0.25	0.13
Fe II 36	b4F-z6Po	5.36	4947.33	0.06	0.06
[Fe II] 20F	a4F-b4F	2.81	4947.37	0.08	0.02
[Fe II] 20F	a4F-b4F	2.86	4950.74	0.10	0.03
[Fe II] 20F	a4F-b4F	2.84	4973.39	0.12	0.03
Fe II 36	b4F-z6Po	5.29	4993.35	0.39	0.21

Table A.2. (continued)

Table A.2. (end)

Line	Transition	ul(eV)	λ (Å)	AAT	WHT	Line	Transition	ul(eV)	λ (Å)	AAT	WHT
[Fe II] 20F	a4F-b4F	2.83	5005.51	0.09	0.02	[N II] 3F	1D-1S	4.05	5754.57	0.24	0.08
Fe II 42	a6S-z6Po	5.36	5018.43	0.56	0.33	Fe II	c4F-y2Ho	8.37	5759.14	n	0.02
[Fe II] 20F	a4F-b4F	2.86	5020.23	0.10	0.03	Fe II	6P-4Po	12.57	5888.34	0.11	0.05
[Fe II] 20F	a4F-b4F	2.84	5043.52	0.06	0.02	Cr II	a2D-z6Po	6.01	5894.65	n	0.01
[Fe II]	a2G-b2D	4.48	5060.08	0.04	0.02	Si II 4	2Po-2S	12.15	5957.56	0.04	0.02
Ti II 113	c2D-x2Do	5.57	5072.28	0.21	0.06	Fe II	p4Go-4d4F	13.24	5977.62	n	0.01
[Fe II] 19F	a4F-a4H	2.68	5072.39	0.01	0.01	Fe II	f4D-4Po	12.59	5985.28	n	0.01
Fe II	c4P-x4Po	8.57	5101.80	0.28	0.07	Fe II] 46	a4G-z6Fo	5.22	5991.38	0.13	0.07
[Fe II] 18F	a4F-b4P	2.78	5107.94	0.05	0.03	Fe II]	e6F-2Go	12.36	5995.51	0.11	n
[Fe II] 19F	a4F-a4H	2.66	5111.63	0.07	0.04	Fe II]	z6Fo-d2G	7.27	5999.48	n	0.01
[Fe II] 18F	a4F-b4P	2.70	5158.00	0.12	0.08	Fe II]	y6Fo-4d4F	12.92	6027.10	n	0.02
[Fe II] 19F	a4F-a4H	2.63	5158.78	0.36	0.19	Fe II]	y4Fo-e6D	9.76	6031.79	0.05	0.02
Fe II] 35	b4F-z6Fo	5.26	5161.18	0.23	0.12	Fe II] 46	a4G-z6Fo	5.33	6044.53	0.03	n
Fe II 42	a6S-z6Po	5.29	5169.03	0.51	0.32	Fe II 200	c4F-x4Fo	8.25	6078.68	n	0.02
[Fe II] 18F	a4F-b4P	2.78	5181.95	0.07	0.04	Fe II] 46	a4G-z6Fo	5.24	6084.11	0.14	0.04
[Fe II] 19F	a4F-a4H	2.69	5184.80	0.01	0.00	Fe II 217	x4Do-e4D	9.90	6088.31	n	0.02
Fe II 49	a4G-z4Fo	5.62	5197.57	0.47	0.26	Fe II] 46	a4G-z6Fo	5.22	6129.71	0.05	0.02
[Fe II] 19F	a4F-a4H	2.68	5220.06	0.06	0.03	Fe II]	y6Fo-4d4F	12.92	6136.56	n	0.02
Fe II 49	a4G-z4Fo	5.59	5234.62	0.26	0.23	Fe II 74	b4D-z4Po	5.90	6147.74	0.10	0.04
[Fe II] 19F	a4F-a4H	2.66	5261.62	0.22	0.11	Fe II 74	b4D-z4Po	5.90	6149.26	0.10	0.04
Fe II 48	a4G-z4Do	5.58	5264.80	0.15	0.06	Fe II 200	c4F-x4Fo	8.23	6175.14	n	0.01
[Fe II] 18F	a4F-b4P	2.70	5268.87	0.08	0.05	Fe II	4Po-4P	10.93	6191.77	0.01	0.02
[Fe II] 18F	a4F-b4P	2.58	5273.35	0.22	0.14	Fe II 74	b4D-z4Po	5.88	6238.37	0.08	0.03
Fe II 49	a4G-z4Fo	5.55	5275.99	0.48	0.24	Fe II 74	b4D-z4Po	5.88	6247.55	0.11	0.05
Fe II 41	a6S-z6Fo	5.24	5284.08	0.32	0.20	[O I] 1F	3P-1D	1.97	6300.23	0.23	0.10
[Fe II] 19F	a4F-a4H	2.69	5296.83	0.04	0.02	[O I] 1F	3P-1D	1.97	6363.88	0.08	0.03
Fe II 49	a4G-z4Fo	5.48	5316.61	0.40	0.28	Fe II 200	c4F-x4F	8.18	6305.32	0.02	n
Fe II 48	a4G-z4Do	5.55	5316.78	0.12	0.08	Fe II	z4Do-c4D	7.47	6317.99	0.11	0.05
Fe II 49	a4G-z4Fo	5.55	5325.56	0.20	0.10	Fe II 40	a6S-z6Do	4.84	6369.45	0.05	0.02
[Fe II] 19F	a4F-a4H	2.68	5333.65	0.14	0.08	Fe II	z4Do-c4D	7.49	6383.72	n	0.02
[Fe II] 18F	a4F-b4P	2.70	5347.65	0.02	0.01	Fe II 74	b4D-z4Po	5.82	6416.89	0.14	0.05
Fe II 48	a4G-z4Do	5.51	5362.86	0.51	0.32	Fe II 40	a6S-z6Do	4.82	6432.68	0.16	0.08
Fe II	6P-4[4]o	12.76	5370.28	0.14	0.07	Fe II 74	b4D-z4Po	5.82	6456.38	0.10	0.07
[Fe II] 19F	a4F-a4H	2.69	5376.45	0.12	0.06	Fe II 199	c4F-x4Go	8.13	6482.21	n	0.06
Fe II	e6G-4[4]o	12.25	5379.03	0.26	0.15	Fe II 40	a6S-z6Do	4.79	6516.05	0.39	0.13
[Fe II] 17F	a4F-a2D2	2.64	5412.65	0.09	0.04	[N II]	3P-1D	1.90	6548.10	0.44	0.11
Fe II]	x4Go-e6G	10.42	5417.05	0.04	n	[N II]	3P-1D	1.90	6583.40	1.28	0.34
Fe II 49	a4G-z4Fo	5.48	5425.27	0.29	0.15	Fe II 210	d2G-w2Ho	9.14	6627.24	0.04	0.02
Fe II] 55	b2H-z4Fo	5.55	5432.98	0.17	0.09	Fe II]	a2F-z6Fo	5.25	6656.00	0.03	0.02
[Fe II] 18F	a4F-b4P	2.58	5433.13	0.07	0.04	Fe II]	y2Po-4P	10.93	6664.05	0.06	0.03
[Fe II] 34F	a4D-b2P	3.34	5477.24	0.13	0.05	[S II]	4So-2Do	1.85	6716.40	0.14	0.05
[Fe II] 17F	a4F-a2D2	2.64	5495.82	n	0.02	[S II]	4So-2Do	1.84	6730.80	0.08	0.01
[Fe II] 17F	a4F-a2D2	2.54	5527.34	0.13	0.06	Fe II]	6Do-4d4F	12.92	6728.45	n	0.02
[Fe II] 34F	a4D-b2P	3.34	5527.61	0.04	0.01	[Fe II] 14F	a4F-a2G	1.96	7155.16	0.27	h
Fe II] 55	b2H-z4Fo	5.48	5534.83	0.33	0.15	Fe II	x4Go-e4D	9.90	7164.35	0.15	h
Fe II]	z6Fo-c4D	7.49	5540.48	0.07	n	[Fe II] 14F	a4F-a2G	2.03	7172.00	0.08	h
[Fe II] 18F	a4F-b4P	2.58	5556.29	0.01	0.01	Fe II] 63	b2G-z4Fo	5.48	7221.37	0.17	h
Fe II	v4Do-4d4F	13.01	5558.06	0.06	n	[Ca II] 1F	2S-2D	1.70	7291.50	0.30	h
Fe II]	z6Fo-c4D	7.49	5573.98	0.04	0.06	[Ca II] 1F	2S-2D	1.69	7323.88	0.31	h
[O I] 1F	1D-1S	1.97	5577.35	0.10	n						
Fe II] 55	b2H-z4Fo	5.48	5591.39	0.08	n						
Fe II] 57	a2F-z4Fo	5.62	5657.94	0.21	h						
N II 3	3Po-3D	20.65	5666.64	0.15	h						
N II 3	3Po-3D	20.65	5676.02	0.18	h						
N II 3	3Po-3D	20.67	5679.56	0.02	h						
N II 3	3Po-3D	20.65	5686.21	0.14	h						
Fe II]	6D-4Po	12.57	5741.47	n	0.03						
[Fe II] 34F	a4D-b2P	3.20	5746.97	0.21	0.06						
Fe II	y4Do-e4D	9.96	5750.88	n	0.05						

